Available online at www.sciencedirect.com
SCIENCE DIRECT®
International Journal of Solids and Structures 42 (2005) 2785–2802
INTERNATIONAL JOURNAL OF SOLIDS and STRUCTURES
www.elsevier.com/locate/ijsolstr

Consecutive matrix cracking in contiguous plies of composite laminates

Tomohiro Yokozeki [a,*], Takahira Aoki [b], Takashi Ishikawa [a]

[a] *Advanced Composite Evaluation Technology Center, Institute of Space Technology and Aeronautics, Japan Aerospace Exploration Agency, 6-13-1 Osawa, Mitaka, Tokyo 181-0015, Japan*
[b] *Department of Aeronautics and Astronautics, University of Tokyo, 7-3-1 Hongo, Bunkyo-ku, Tokyo 113-8656, Japan*

Received 5 April 2004; received in revised form 25 September 2004
Available online 5 November 2004

Abstract

Propagation behaviors of obliquely-crossed microcracks induced by matrix cracks in adjacent plies of composite laminates were numerically analyzed using finite element modeling. Oblique coordinate system along obliquely-crossed cracks was defined and applied to the finite element formulation, which enabled geometrically parametric analysis for arbitrary oblique angles using a single discrete model. Three-dimensional stress analyses of $[S/\theta_n/90]s$ laminate with microcracks in θ-ply and fully developed matrix cracks in 90-ply were performed under various conditions of angle θ, θ-ply crack length, θ-ply thickness, etc. Energy release rates associated with θ-ply crack propagation in the θ-ply fiber direction were calculated in order to assess θ-ply cracking conformations. The results suggested that presence of 90-ply cracks affects θ-ply crack propagation, especially mode-I energy release rates, depending on angle θ. Furthermore, effects of angle θ, θ-ply thickness and S layer configuration on the interaction between matrix cracks in θ- and 90-plies were clarified. Finally, crack accumulation behaviors in $[0/\theta_2/90]s$ laminates were experimentally investigated and compared with the analytical results.

Keywords: Laminates; Transverse cracking; Finite element analysis; Oblique coordinate system; Multiple ply crack

1. Introduction

Composite laminates are commonly used as various structures because of the high mechanical performance. However, the observed damage process is rather complex consisting of matrix cracks (or transverse

* Corresponding author. Tel.: +81 422 40 3384; fax: +81 422 40 3549.
E-mail address: yokozeki@chofu.jaxa.jp (T. Yokozeki).

0020-7683/$ - see front matter © 2004 Elsevier Ltd. All rights reserved.
doi:10.1016/j.ijsolstr.2004.09.040

cracks), delaminations, fiber-matrix debondings, fiber fractures, etc. Among them, matrix cracking is often the first observed damage mode under tensile loadings and induces the reduction of laminate thermo-mechanical performance, more severe damages and leakage of contained liquid or gas. Thus, good understanding of the damage process of matrix cracks is necessary for evaluating the performance and durability of composite laminates.

Recently, CFRP (carbon fiber reinforced plastic) laminates have received great attention as the major candidates for reducing the structural weight of future space launch vehicles (Robinson, 1994; Johnson et al., 2004). Particularly, the application of CFRP to the cryogenic propellant tanks is one of the most desired but challenging technologies for achieving the drastic weight reduction. Basic research on the feasibility of cryogenic composite propellant tanks indicates that matrix crack onset and its accumulation are inevitable when applying the conventional high performance composites to the cryogenic tanks and through-thickness connection of matrix cracks induces crucial propellant leakage (Aoki et al., 2000; Kumazawa et al., 2003). Because of this, the damage process of matrix crack accumulation has to be clarified from the viewpoint of the cryogenic composite tank design.

Matrix cracking in off-axis plies of composite laminates under static and fatigue loadings has been extensively studied. Several analytical models to predict effective properties and stress/strain field of laminates with fully propagating matrix cracks have been developed (Garrett and Bailey, 1977; Hashin, 1985; McCartney, 1992; Schoeppner and Pagano, 1998) and summarized in the review articles (Nairn and Hu, 1994; Nairn, 2000). Also, experimental works on damage accumulation in composite laminates have been actively engaged in the last two or three decades (Garrett and Bailey, 1977; Flagg and Kural, 1982; Highsmith and Reifsnider, 1982; Ogin et al., 1985; Takeda and Ogihara, 1994; Nairn and Hu, 1994; Nairn, 2000). These comprehensive researches led to the better understanding and correlation between the predictions and experiments of the damage accumulation in the first cracked layers, especially in 90° layers.

Contrary to the above-mentioned first ply cracking, crack accumulation in multiple plies of composite laminates has not been well understood. Although experimental studies on crack density history in multiple plies during static or fatigue loading (Masters and Reifsnider, 1982; McManus and Maddocks, 1996; Tong et al., 1997) or crack-induced microcracks (Johnson and Chang, 2001; Lavoie and Adolfsson, 2001) and overall stiffness analysis of laminates with multiple ply cracks using equivalent or homogenization method (Gudmundson and Zang, 1993; McManus and Maddocks, 1996; Zhang and Herrmann, 1999; McCartney, 2003) have been performed, detailed researches on the damage accumulation process of multiple ply cracks were rarely reported. Two- or three-dimensional stress analyses of orthogonally-cracked laminates (e.g. $[0_m/90_n]$s with matrix cracks in both layers) exist (Hashin, 1987; Aboudi et al., 1988; Tsai and Daniel, 1993; Henaff-Gardin et al., 1996; Kashtalyan and Soutis, 2000) and synergistic effects of multiple ply cracks and stress distribution at the vicinity of crack intersection were discussed. However, detailed mechanism of multiple ply crack accumulation (e.g. how transverse cracks evolve and propagate in the fiber direction in adjacent plies of cracked layers) in general laminates is further to be investigated.

The scope of this study is to investigate microcracking behaviors induced by matrix cracks in adjacent ply in order to clarify the multiple ply cracking mechanisms in composite laminates. A parametrically oriented methodology for stress analysis of laminated structures containing of obliquely-crossed transverse cracks is introduced based on an oblique coordinate system and applied to the finite element formulation. Using displacement/strain covariant components and force/stress contravariant components, equivalence that obliquely-crossed crack problem can be transformed to orthogonally-crossed crack problem is revealed, which permits geometrically parametric stress analysis utilizing a single discrete model. $[S/\theta_n/90]$s laminates with microcracks in θ-ply and fully developed matrix cracks in 90-ply are analyzed under various conditions of angle θ, θ-ply crack length, θ-ply thickness, etc. Effects of angle θ, θ-ply thickness and S layer configuration on the susceptibility of micro-formed or developed θ-ply cracks are discussed by calculating energy release rates associated with θ-ply crack growth in the fiber direction. Finally, crack accumulation behaviors in $[0/\theta_2/90]$s laminates are experimentally investigated and compared with the analytical results.

2. Analytical modeling

2.1. Oblique coordinate system

Consider a $[S/\theta_m/90_n]s$ laminate containing obliquely-crossed cracks, i.e. θ- and 90-ply cracks. In order to discuss stress distributions and boundary settings, it is spontaneous to utilize the oblique coordinate system along θ- and 90-ply cracks. Let r_1 and r_2 denote reference lines along θ- and 90-ply fiber directions respectively. The base vectors $\mathbf{g}_1$, $\mathbf{g}_2$ and $\mathbf{g}_3$ are set along r_1, r_2 and the line perpendicular to the plane including r_1 and r_2 respectively as shown in Fig. 1, while the contravariant base vectors $\mathbf{g}^i$ can be defined with the reciprocal relationship between these vectors. On the other hand, unit base vectors of orthogonal coordinate system along 0- and 90-ply fiber direction utilized in the common stress analysis are defined as $\mathbf{i}_1$, $\mathbf{i}_2$ and $\mathbf{i}_3$ as shown in Fig. 1. The coordinate systems based on $\mathbf{g}_i$ and $\mathbf{i}_i$ are denoted as x–y–z oblique coordinates and $\bar{x}$–$\bar{y}$–$\bar{z}$ orthogonal coordinates respectively. In this study, base vectors $\mathbf{g}_i$ are set so that all contravariant base vectors $\mathbf{g}^i$ have the unit length, which permits parametric analysis for angle θ under the conditions of constant oblique crack densities.

The covariant base vectors $\mathbf{g}_i$ are expressed in terms of orthogonal coordinate components as

$$\begin{aligned}\mathbf{g}_1 &= (1, \tan\theta, 0)\\ \mathbf{g}_2 &= (0, \sec\theta, 0)\\ \mathbf{g}_3 &= (0, 0, 1)\end{aligned} \tag{1}$$

Relationship between oblique coordinate components and orthogonal coordinate components of vectors and tensors can be derived straightforward. In this study, displacement/strain covariant components and force/stress contravariant components are applied to the formulation because of the symmetry characteristics and compatibility to the physical work or energy. The derived relationship between the corresponding oblique coordinate components and orthogonal coordinate components are presented in Appendix A. In this paper, subscripts, superscripts and overbar denote covariant and contravariant components in oblique coordinates and orthogonal components respectively. The matrix form notation is expressed by [ ], in which summation convention is not employed.

2.2. Finite element formulation

The virtual work principal is expressed in terms of matrix-formed oblique coordinate components with application of constitutive equation including initial strains $\boldsymbol{\varepsilon}^0$ as

$$\int_V \delta[\varepsilon_{ij}]^{\mathrm{T}}[Q^{ijkl}]\{[\varepsilon_{ij}] - [\varepsilon_{ij}^0]\}\mathrm{d}V = \int_{S_{\mathrm{F}}} \delta[u_i]^{\mathrm{T}}[F^i]\mathrm{d}S + \int_V \delta[u_i]^{\mathrm{T}}[X^i]\mathrm{d}V \tag{2}$$

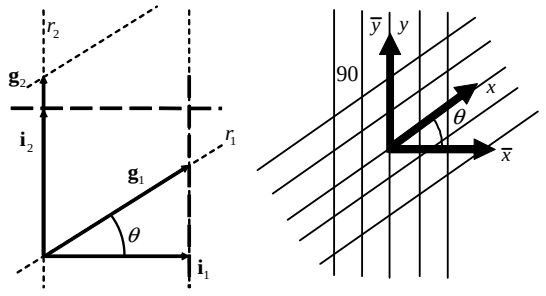

Fig. 1. Orthogonal and oblique coordinate system.

where V, S and S_F denote the volume, the whole surface and the traction-loaded boundaries of the body respectively. In addition, $\mathbf{X}$ and $\mathbf{F}$ represent the body force and the prescribed boundary tractions. Also,

$$[Q^{ijkl}] = [T]^{-T}[\overline{Q}][T]^{-1} \tag{3}$$

is the fourth order contravariant components of stiffness tensor in oblique coordinates in matrix form and $[T]$ based on the base vectors of Eq. (1) is given in Appendix A.

Following the common finite element formulation, the element stiffness equation can be obtained as

$$[K^{(m)}][d_i^{(m)}] = [F_0^{(m)}] + [F_S^{(m)}] + [F_V^{(m)}] \equiv [F^{(m)}] \tag{4}$$

where m is the element index and

$$\begin{aligned} [K^{(m)}] &= \int_{V^{(m)}} [B]^T [Q^{ijkl}][B] \mathrm{d}V, \quad [F_0^{(m)}] = \int_{V^{(m)}} [B]^T [Q^{ijkl}][\varepsilon_{ij}^0] \mathrm{d}V \\ [F_S^{(m)}] &= \int_{S_F^{(m)}} [N]^T [F^i] \mathrm{d}S, \quad [F_V^{(m)}] = \int_{V^{(m)}} [N]^T [X^i] \mathrm{d}V \end{aligned} \tag{5}$$

where $[N]$ and $[d_i^{(m)}]$ denote interpolated functions and nodal displacements. $[B]$ is given by the covariant derivative operation of $[N]$ using displacement–strain relationship. The global stiffness equation follows the superposition of each element equation as in the conventional finite element formulation.

However, integrals over volume or area should be noted. The volume integral can be rewritten as

$$\int_V \mathrm{d}V = \iiint \sqrt{g}\, \mathrm{d}x\, \mathrm{d}y\, \mathrm{d}z \tag{6}$$

where g is the determinant of covariant metric tensor matrix. Also, the area integral over stress-prescribed boundaries can be expressed as

$$\begin{aligned} \int_S F^i \mathrm{d}S &= \iint \sigma^{1i} n_1 \sqrt{g \cdot g^{11}}\, \mathrm{d}y\, \mathrm{d}z + \iint \sigma^{2i} n_2 \sqrt{g \cdot g^{22}}\, \mathrm{d}x\, \mathrm{d}z + \iint \sigma^{3i} n_3 \sqrt{g \cdot g^{33}}\, \mathrm{d}x\, \mathrm{d}y \\ &= \iint \sigma^{1i} \hat{n}_1 \sqrt{g}\, \mathrm{d}y\, \mathrm{d}z + \iint \sigma^{2i} \hat{n}_2 \sqrt{g}\, \mathrm{d}x\, \mathrm{d}z + \iint \sigma^{3i} \hat{n}_3 \sqrt{g}\, \mathrm{d}x\, \mathrm{d}y \end{aligned} \tag{7}$$

Here, $\hat{n}_i = n_i \sqrt{g^{ii}}$ are physical components of normal vectors (summation on i is precluded) and g^{ij} are contravariant metric tensor component. These results suggest that there is no need of correction in the stiffness Eq. (4) when using physical normal vector components as the compensation terms $\sqrt{g}$ are counteracted. Note that, in this case, covariant components of the applied concentrated loads should be divided by $\sqrt{g}$ as input values.

The above-mentioned results provide the insight that the problem with oblique geometry having arbitrary oblique angles can be transformed to the orthogonal shaped problem as shown in Fig. 2, when utilizing covariant displacement/strain components, contravariant force/stress components and associated stiffness components. A geometrical model with any oblique angle can be analyzed using the corresponding orthogonal one. After solving the orthogonal problem incorporating transformed components of stiffness and boundary conditions, reverse transformation of the obtained components results in the solution of the oblique problem. This methodology has no restriction on the whole structural geometries or the selection of the base vectors, and exhibits the potential of geometrically parametric stress analysis utilizing a single discrete model.

In this paper, in-plane oblique coordinate system was introduced for the analysis of obliquely-crossed cracks in contiguous plies. However, any true 3D oblique coordinate system, whose three base vectors intersect obliquely each other, is easily applicable to this formulation. Moreover, this formulation does not depend on choice of base vectors. Also, any other analytical methods may be combined with the present

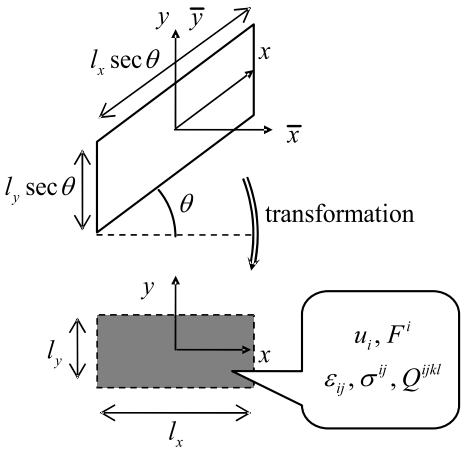

Fig. 2. Transformation of obliquely crossed problem to orthogonally crossed problem with oblique coordinate components.

scheme as described by Yokozeki and Aoki (2004), which presented two-dimensional shear-lag analysis of laminates containing obliquely-crossed cracks.

2.3. Stress analysis of laminates with obliquely-crossed cracks

[S/θ_n/90]s laminates containing θ- and 90-ply cracks are analyzed utilizing the transformation modeling. It is assumed that: (1) 90-ply cracks propagate completely in the fiber direction and are regularly distributed with crack density of ρ_2; (2) θ-ply cracks are symmetrically arranged with respect to the central plane, all of which have length $2a\sec\theta$ (projected length $2a$) propagating equally in the fiber direction from the 90-ply crack tips and uniform crack density of ρ_1; (3) The θ-ply crack tips are straight along the thickness direction. Configuration of the assumed model is shown in Fig. 3(a). Thus, the representative volume to be analyzed can be taken as Fig. 3(b) and geometrically modeled in the orthogonal shape as Fig. 3(c), in which covariant displacement/strain components, contravariant force/stress components and the related stiffness are applied. The model with orthogonal geometry can be used for any angle θ under the conditions of constant crack densities.

In the model of Fig. 3(c), boundary conditions at the corresponding nodes on the surfaces across x and y axes should be applied as

$$\begin{cases} u^{A_1} - u^{A_2} = \varepsilon_x l_x, \quad v^{A_1} - v^{A_2} = \gamma_{xy} l_x, \quad w^{A_1} - w^{A_2} = 0 \\ u^{B_1} - u^{B_2} = 0, \quad v^{B_1} - v^{B_2} = \varepsilon_y l_y, \quad w^{B_1} - w^{B_2} = 0 \end{cases} \tag{8}$$

where ε_{ij} is the prescribed covariant strain components, A_i and B_i are the boundary surfaces defined in Fig. 3(c) and l_x and l_y are equal to $1/\rho_2$ and $1/\rho_1$ respectively. Note that the oblique coordinate formulation permits tractable expression of the periodic boundary conditions for obliquely-crossed problem.

In the present study, θ-ply crack propagation process beyond the accumulation of transverse cracks in 90-ply is the major concern. Transverse cracks in one layer may induce cracks in the adjacent plies under static or fatigue loadings in the form of microcracks as reported by Johnson and Chang (2001) and Lavoie and Adolfsson (2001). Therefore, energy release rates associated with θ-ply crack propagation are calculated using results of three-dimensional stress analysis based on the present formulation. The detailed procedure for calculating energy release rates using oblique coordinate components is given in Appendix B. The case of $\rho_1 = 5\,\mathrm{cm}^{-1}$ and $\rho_2 = 2\,\mathrm{cm}$ is only examined in this calculation. Eight-node isoparametric elements are used in this study. Double nodes are arranged in the crack surfaces and θ-ply crack length

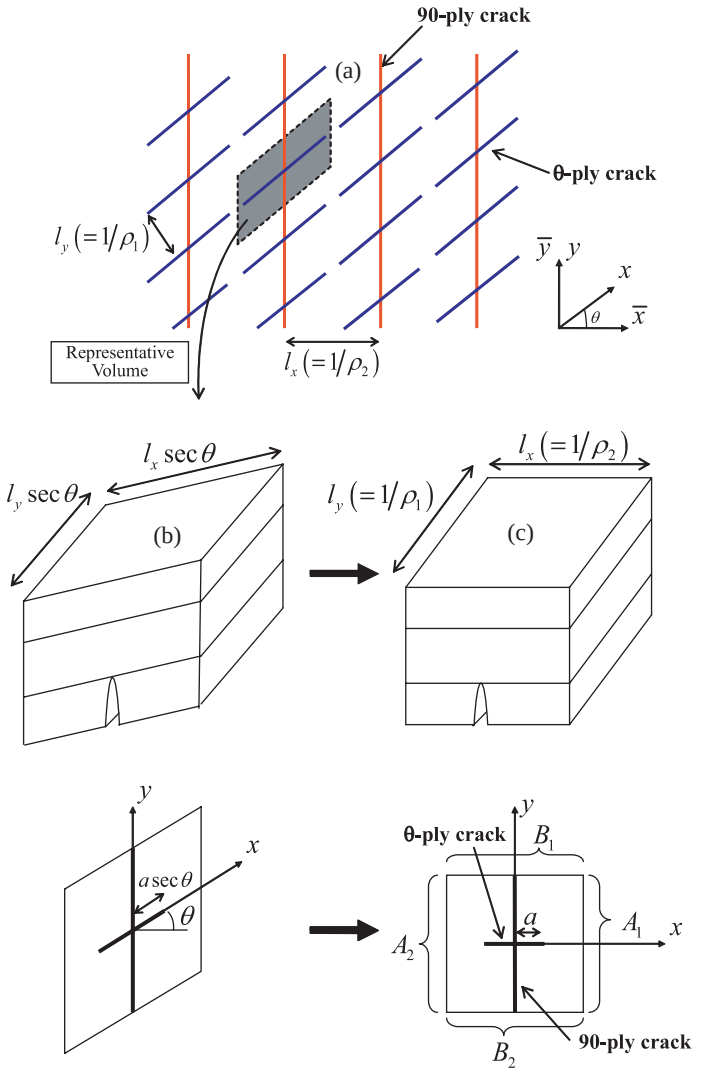

Fig. 3. [S/θ_2/90]s laminate model containing θ- and 90-ply cracks: (a) whole model containing periodic arrays of obliquely-crossed cracks; (b) representative volume model; (c) transformed model.

is controlled by fixing the corresponding double nodes. Ply thickness is set to be 0.14 mm and material properties used here are summarized in Table 1 in reference to Aoki et al. (2000). It should be noted that

Table 1
Material properties used in the analysis (Aoki et al., 2000)

Temp. (°C)	E_L (GPa)	E_T (GPa)	ν_{LT}	G_{LT} (GPa)	G_{TT} (GPa)	α_L (μ/°C)	α_T (μ/°C)
100	146.4	6.28	0.359	2.15	2.16	−0.60	41.5
60	146.8	7.24	0.354	3.53	2.50	−0.45	36
20	147.1	8.31	0.352	4.71	2.87	−0.55	22.5

ν_{TT} is assumed to be 0.45.

temperature dependence of material properties is included using linear interpolation between the given temperatures and stress-free and setting temperatures are assumed to be 100 and 20 °C. Although delaminations may be induced at the vicinity of obliquely-crossed cracks, they are assumed to evolve beyond the θ-ply crack propagation. Therefore, effect of delaminations on θ-ply crack propagation is neglected in this study.

3. Numerical results

In this section, crack propagation behavior induced by transverse cracks in the adjacent plies is clarified using the finite element model described in Section 2.3 based on oblique coordinate formulation. Effects of some controlling parameters (stacking configuration, applied strains, etc.) on θ-ply crack conformation of $[S/\theta_n/90]s$ laminate containing fully developed 90-ply transverse cracks are assessed in the following sections.

3.1. Effect of angle θ on θ-ply crack conformation

$[0/\theta_2/90]s$ laminates with obliquely-crossed cracks in contiguous θ- and 90-plies are considered here. The analyses were performed under the conditions of uniaxial tension loadings in the 0° direction corresponding to $\bar{\varepsilon}_x = 1.0\%$ (orthogonal components). Calculated energy release rates are plotted as a function of normalized projected crack length (projected length a divided by θ-ply thickness) in Fig. 4 in the cases of $\theta = 30°$ and 60°. For comparison, the values associated with θ-ply crack growth without 90-ply cracks are also

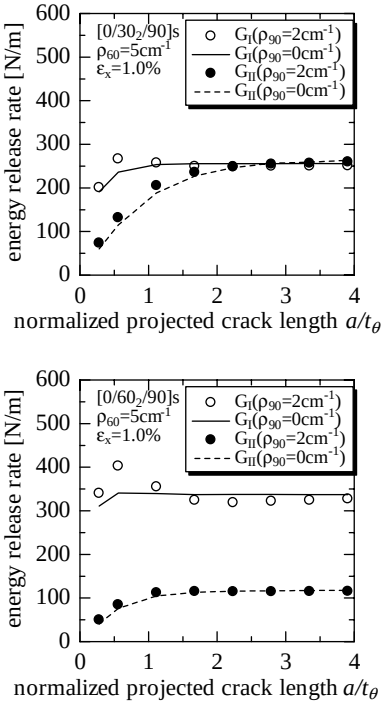

Fig. 4. Energy release rates associated with θ-ply crack propagation as a function of normalized projected crack length in $[0/\theta_2/90]s$ laminates with $\theta = 30°$ and 60° compared with the case without 90-ply cracks.

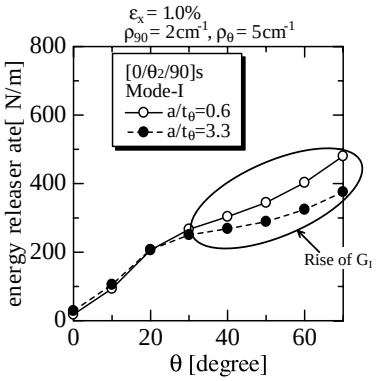

Fig. 5. Parametric analysis of maximum and saturated energy release rates associated with θ-ply crack growth in $[0/\theta_2/90]$s laminates.

shown. It can be seen that mode-I energy release rates increase at the vicinity of 90-ply cracks due to the existence of 90-ply cracks, whereas mode-II components are barely influenced. When crack length increases, energy release rates reach the steady state, which is common between the cases with and without 90-ply cracks. In addition, difference of mode-I components between the maximum and saturated values becomes large in conjunction with angle θ increase. Mode-I energy release rates in the cases of projected crack length $a/t_\theta = 0.6$ (indicating the maximum values G_{Imax}) and $a/t_\theta = 3.3$ (indicating the saturated values G_{Isat}) are plotted as a function of θ in Fig. 5, implying that mode-I components rise in the case of $a/t_\theta = 0.6$ is recognized for large θ. In the case of θ close to 0°, energy release rate distribution has no peak at the vicinity of 90-ply cracks in contrast to the cases as shown in Fig. 4. Thus, G_{Imax} is defined as the value at $a/t_\theta = 0.6$, which means that $G_{\mathrm{Imax}}/G_{\mathrm{Isat}}$ may have values lower than unity. Large difference between the increased and saturated mode-I energy release rates causes arrested cracks or micro-formed cracks under constant prescribed strains as shown in Fig. 6. Therefore, the above-mentioned results indicate that:

(1) 90-ply cracks have significant effects on θ-ply cracking behavior especially in the case of large angle θ.
(2) Mode-I energy release rates associated with θ-ply crack growth are mainly influenced by 90-ply cracks.

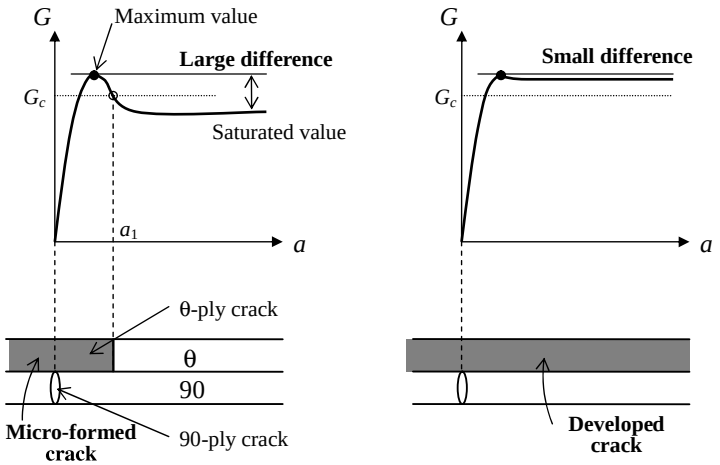

Fig. 6. Schematics of the relationship between crack length and energy release rate rise.

(3) When microcracks in θ-ply appear from 90-ply crack tips, they propagate slightly in the case of large θ because of the large difference between the maximum and saturated mode-I energy release rates, which causes observation of micro-formed θ-ply cracks.
(4) Micro-formed θ-ply cracks are recognized only when difference angle between the cracked and adjacent plies is small (or θ is larger than 40° or 50°), otherwise only developed cracks may be observed.

It should pointed out that matrix cracking under mixed-mode loading may be evaluated with consideration of mode-I and mode-II energy release rates. However, mode-II components have relatively low values compared with mode-I components within the examples in this study and mode-II fracture toughness is several times higher than mode-I toughness in the case of polymer based composites. Therefore, mode-I components are used for discussions on the matrix cracking behaviors.

3.2. Effect of θ-ply thickness on θ-ply crack conformation

Energy release rate ratios $G_{\mathrm{Imax}}/G_{\mathrm{Isat}}$ of $[0/\theta/90]$s laminates with obliquely-crossed cracks were also calculated under uniaxial tension loadings in the 0° direction corresponding to $\bar{\varepsilon}_x = 1.0\%$. Comparison of energy release rate ratios as a function of angle θ between $[0/\theta/90]$s and $[0/\theta_2/90]$s laminates is given in Fig. 7, indicating significant effect of θ-ply thickness on θ-ply crack conformation. Thus, it is concluded that micro-formed cracks are susceptible to initiation in thinner adjacent plies because of the higher difference of energy release rates.

3.3. Effect of applied strains on θ-ply crack conformation

In order to investigate the applied strain level on difference of energy release rates, energy release rate ratios $G_{\mathrm{Imax}}/G_{\mathrm{Isat}}$ (G_{I} at $a/t_\theta = 0.6$ divided by G_{I} at $a/t_\theta = 3.3$) were calculated for the cases of $\bar{\varepsilon}_x = 1.0\%$, $\bar{\varepsilon}_y = R\bar{\varepsilon}_x$ and $\bar{\gamma}_{xy} = 0\%$ (R is varied) with some variety of angle θ as shown in Fig. 8. Although applied strains have some effects on the energy release rate difference, the trend of θ dependence is almost same (larger θ causes larger difference). Therefore, the susceptibility of micro-formed adjacent-ply cracks (instead of propagation along the fiber direction) proves to have dependence mainly on geometry, i.e. angle θ or difference angle between the contiguous plies.

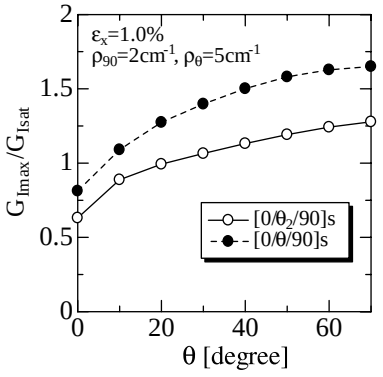

Fig. 7. Effect of θ-ply thickness on the energy release rate ratio $G_{\mathrm{Imax}}/G_{\mathrm{Isat}}$.

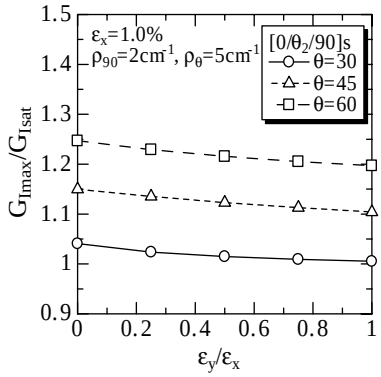

Fig. 8. Effect of applied strains on the energy release rate ratio $G_{\mathrm{Imax}}/G_{\mathrm{Isat}}$.

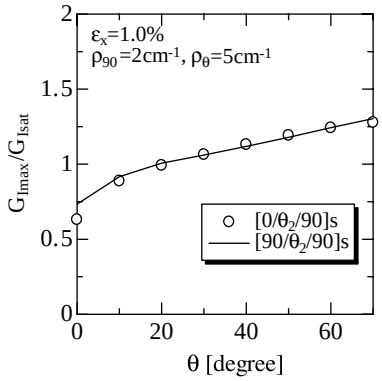

Fig. 9. Effect of the intact S-layer configuration on the energy release rate ratio $G_{\mathrm{Imax}}/G_{\mathrm{Isat}}$.

3.4. Effect of S layer on θ-ply crack conformation

In order to assess the constraint effect of the intact S layer on θ-ply crack conformation, calculated energy release rate ratios $G_{\mathrm{Imax}}/G_{\mathrm{Isat}}$ of $[90/\theta_2/90]$s laminates are plotted in Fig. 9 as a function of angle θ, compared with the case of $[0/\theta_2/90]$s laminates. Applied strain conditions were same as the described ones in Sections 3.1 and 3.2. Energy release rate ratios have almost identical values for any θ, although some difference is identified in the case of small θ ($\theta < 10°$), which may be due to error in calculating the ratios using small energy release rate values. Therefore, the intact S layer has little effect on θ-ply crack conformation.

4. Experimental

4.1. Materials and methods

In order to verify the mechanisms of matrix cracking in contiguous plies, experimental investigation of $[0/\theta_2/90]$s laminates analyzed in the previous section is provided. Especially, crack accumulation process in θ-ply in the presence of 90-ply cracks is focused on.

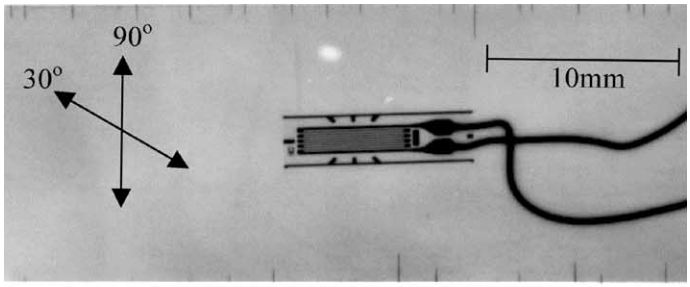

(a) σ_x=401[MPa]、 ε_x=0.80%

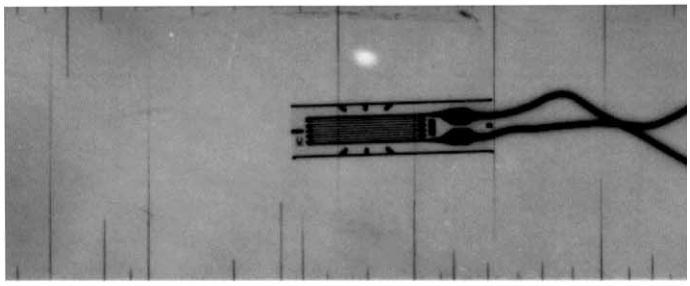

(b) σ_x=449[MPa]、 ε_x=0.90%

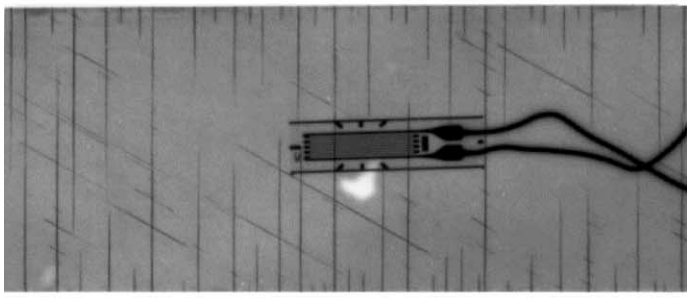

(c) σ_x=491[MPa]、 ε_x=1.00%

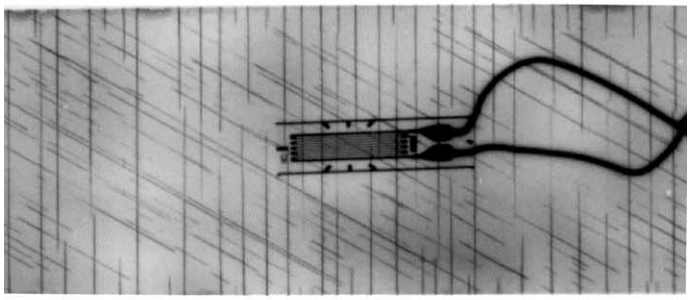

(d) σ_x=531[MPa]、 ε_x=1.10%

Fig. 10. Consecutive matrix cracking behaviors in contiguous plies in a $[0/30_2/90]$s laminate.

Three types of coupon specimens of $[0/30_2/90]$s, $[0/45_2/90]$s and $[0/60_2/90]$s were prepared. The material system is IM600/#133, intermediate modulus carbon fiber and toughened epoxy system. All specimens were 250 mm long with 50 mm GFRP end-tabs leaving a 150 mm gauge section. Due to the shear-extension coupling of the whole laminate characteristics, specimen width was configured to be 15 mm in order to assure enough regions of uniform deformation.

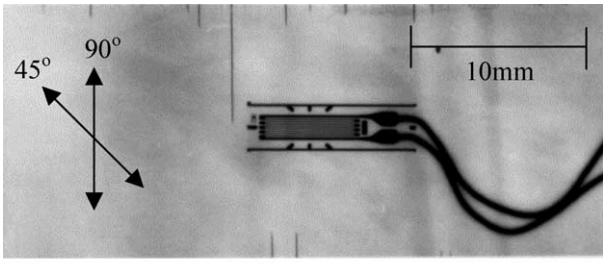

(a) σ_x=351[MPa]、 ε_x=0.74%

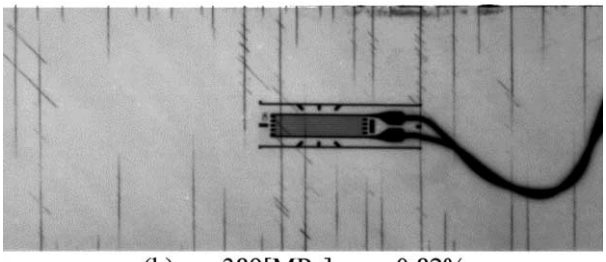

(b) σ_x=389[MPa]、 ε_x=0.82%

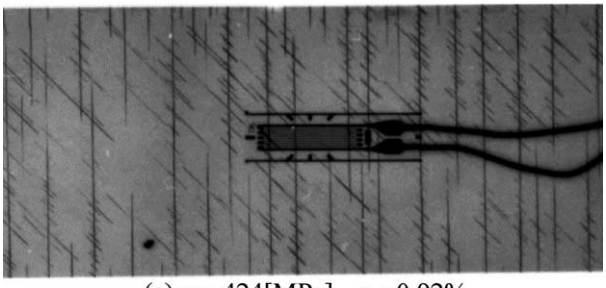

(c) σ_x=424[MPa]、 ε_x=0.92%

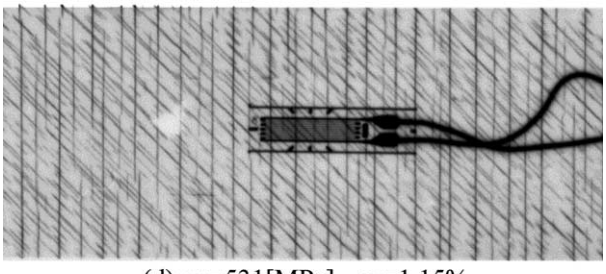

(d) σ_x=531[MPa]、 ε_x=1.15%

Fig. 11. Consecutive matrix cracking behaviors in contiguous plies in a $[0/45_2/90]$s laminate.

Quasi-static tensile tests were performed using Instron8802 hydraulic driven loading machine at cross-head speed of 0.5 mm/min at room temperature. Strain gauges were attached to the specimens for measuring axial strains. Soft X-ray radiography was applied to the cracked specimens using zinc iodide penetrant in order to check cracking patterns.

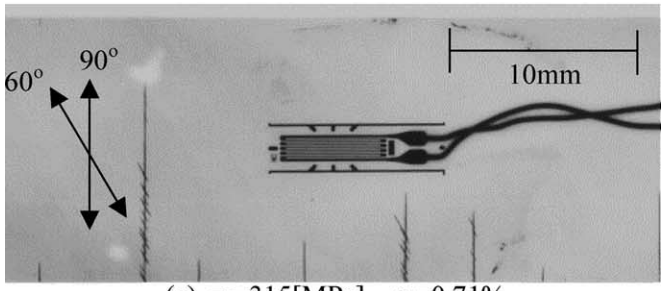

(a) σ_x=315[MPa]、 ε_x=0.71%

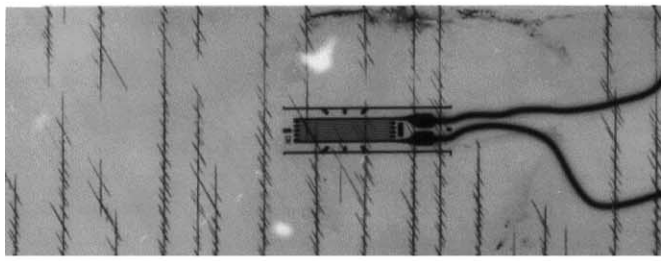

(b) σ_x=347[MPa]、 ε_x=0.80%

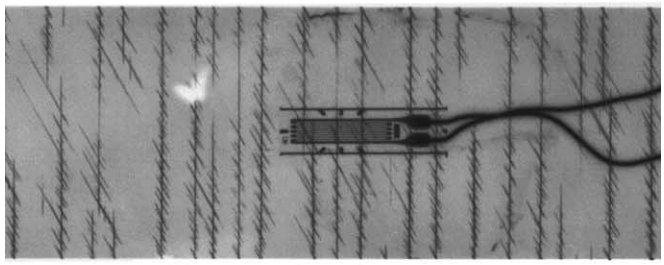

(c) σ_x=388[MPa]、 ε_x=0.89%

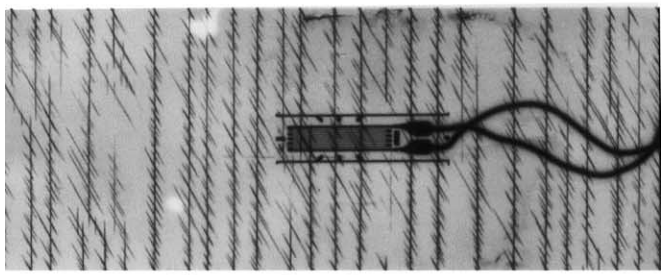

(d)σ_x=428[MPa]、 ε_x=1.00%

Fig. 12. Consecutive matrix cracking behaviors in contiguous plies in a $[0/60_2/90]$s laminate.

4.2. Results and discussion

In Figs. 10–12, θ-ply cracking configuration is shown in the presence of 90-ply cracks for $\theta = 30°$, 45° and 60°. It should be pointed out that micro-formed θ-ply cracks with high density could be observed in $[0/45_2/90]$s and $[0/60_2/90]$s laminates when 90-ply cracks initiated and extended in the fiber direction. At higher strain level, micro-formed cracks increased in number in conjunction with 90-ply crack increase. In contrast, micro-formed cracks were rarely observed in $[0/30_2/90]$s laminates and 30-ply cracks appeared as developed cracks. These results indicate that intersecting angle between the contiguous cracked plies (i.e. 90- and θ-ply) has significant effects on the process of θ-ply crack formation. When the intersecting angle is small, micro-formed cracks are observed before propagation in the fiber direction as the cases of $\theta = 45°$ and 60°. However, developed cracks mainly form in the cases of large intersecting angles.

In the analytical investigation, energy release rates associated with θ-ply crack growth in the presence of fully developed 90-ply cracks were discussed and difference between the increased and the saturated mode-I components was notified. The large difference causes the stable growth of θ-ply crack, leading to the observation of micro-formed cracks, whereas small difference indicates the unstable growth once microcracks occur, which results in the formation of developed cracks. This investigation coincides well with the experimental observation. Layup geometry proved to affect the damage process of matrix cracking in multiple plies. This finding reveals the possibility of controlling the damage accumulation process using optimized layup or geometry.

As mentioned in Introduction, through-thickness connection of matrix cracks provokes the serious fuel leakage of composite tanks. In general composite laminates, developed cracks as well as micro-formed cracks are expected to accumulate in multiple plies under complex thermo-mechanical loadings. Because the amount of leakage is affected by the size of damage contained in composites laminates, the mechanisms of matrix crack accumulation have great impact on the leakage problem. Although the relation of matrix cracking to the propellant leakage has to be further investigated, this study provides the insight into the dominant damage mode induced by matrix cracks in the adjacent plies.

5. Concluding remarks

Microcracking behaviors induced by matrix cracks in the adjacent plies were analytically investigated in order to clarify cracking mechanisms in multiple plies of composite laminates. For the parametrically oriented finite element modeling, oblique coordinate system along obliquely-crossed cracks was defined. Displacement/strain covariant components and force/stress contravariant components were applied to the finite element formulation, which enabled geometrically parametric analysis for arbitrary oblique angles using a single orthogonally-shaped discrete model.

Three-dimensional stress analyses of $[S/\theta_n/90]$s laminates with microcracks in θ-ply and fully developed matrix cracks in 90-ply were performed under various conditions of angle θ, θ-ply crack length, θ-ply thickness and S layer layup. Calculation of energy release rates associated with θ-ply crack growth led to the following results.

(i) Matrix cracks in 90-ply have significant effects on energy release rates (especially mode-I), thus θ-ply cracking behavior.
(ii) Mode-I energy release rates associated with θ-ply crack growth shows the maximum values at the vicinity of 90-ply crack tips and decreases to the saturated values in conjunction with increase of θ-ply crack length. Large difference between the maximum and saturated values causes observation of micro-formed θ-ply cracks.

(iii) Difference between the maximum and saturated energy release rates, or the ratio $G_{\mathrm{Imax}}/G_{\mathrm{Isat}}$ is large in the case of small difference angle between the cracked contiguous plies (θ- and 90-plies).
(iv) Thickness of θ-ply proves to significantly control θ-ply crack conformation. Micro-formed cracks are susceptible to initiation in thin θ-ply because of the large difference of energy release rates.
(v) Applied strains or configurations of the intact S-layer have little effect on the ratio $G_{\mathrm{Imax}}/G_{\mathrm{Isat}}$. The susceptibility of micro-formed adjacent-ply cracks have dependence mainly on difference angle between the cracked contiguous plies and θ-ply thickness, i.e. geometrical conditions.

Crack accumulation in multiple plies of $[0/\theta_2/90]$s laminates ($\theta = 30°$, 45° and 60°) was experimentally investigated. Micro-formed θ-ply cracks were induced by 90-ply cracks in the cases of $\theta = 45°$ and 60°, whereas developed 30-ply cracks were mainly recognized in $[0/30_2/90]$s laminates. The intersecting angle between the contiguous cracked plies proved to have significant effects on the process of θ-ply crack formation, which coincided well with analytical investigation.

Appendix A

Covariant components of displacement vectors and strain tensors are utilized in this study, whereas contravariant components of force vectors and stress tensors are applied as mentioned in Section 2.1. When covariant base vectors given in Eq. (1) are utilized, transformations from orthogonal components to oblique components are as follows.

Displacement (*covariant*)

$$[u_i] = \begin{bmatrix} 1 & \tan\theta & 0 \\ 0 & \sec\theta & 0 \\ 0 & 0 & 1 \end{bmatrix} [\bar{u}] \equiv [Z][\bar{u}] \tag{A.1}$$

Force (*contravariant*)

$$[F^i] = \begin{bmatrix} 1 & 0 & 0 \\ -\sin\theta & \cos\theta & 0 \\ 0 & 0 & 1 \end{bmatrix} [\overline{F}] \equiv [Z]^{-\mathrm{T}}[\overline{F}] \tag{A.2}$$

Strain (*covariant*)

$$[\varepsilon_{ij}] = \begin{bmatrix} 1 & \tan^2\theta & 0 & 0 & 0 & \tan\theta \\ 0 & \sec^2\theta & 0 & 0 & 0 & 0 \\ 0 & 0 & 1 & 0 & 0 & 0 \\ 0 & 0 & 0 & \sec\theta & 0 & 0 \\ 0 & 0 & 0 & \tan\theta & 1 & 0 \\ 0 & 2\sec\theta\tan\theta & 0 & 0 & 0 & \sec\theta \end{bmatrix} [\bar{\varepsilon}] \equiv [T][\bar{\varepsilon}] \tag{A.3}$$

Stress (*contravariant*)

$$[\sigma^{ij}] = \begin{bmatrix} 1 & 0 & 0 & 0 & 0 & 0 \\ \sin^2\theta & \cos^2\theta & 0 & 0 & 0 & -2\cos\theta\sin\theta \\ 0 & 0 & 1 & 0 & 0 & 0 \\ 0 & 0 & 0 & \cos\theta & -\sin\theta & 0 \\ 0 & 0 & 0 & 0 & 1 & 0 \\ -\sin\theta & 0 & 0 & 0 & 0 & \cos\theta \end{bmatrix} [\bar{\sigma}] \equiv [T]^{-\mathrm{T}}[\bar{\sigma}] \tag{A.4}$$

Oblique components of the above-mentioned matrices are given by

$$\begin{aligned} [u_i] &= [\, u_x \quad u_y \quad u_z \,]^{\mathrm{T}} \\ [F^i] &= [\, F^x \quad F^y \quad F^z \,]^{\mathrm{T}} \\ [\varepsilon_{ij}] &= [\, \varepsilon_x \quad \varepsilon_y \quad \varepsilon_z \quad \gamma_{yz} \quad \gamma_{xz} \quad \gamma_{xy} \,]^{\mathrm{T}} \\ [\sigma^{ij}] &= [\, \sigma^x \quad \sigma^y \quad \sigma^z \quad \tau^{yz} \quad \tau^{xz} \quad \tau^{xy} \,]^{\mathrm{T}} \end{aligned} \tag{A.5}$$

and correspondingly for orthogonal components.

Appendix B

Procedure of calculating energy release rates using crack closure method is presented herein. A magnified plan view at the vicinity of crack tip in the θ-ply fiber direction is shown in Fig. 13. Crack opening displace-

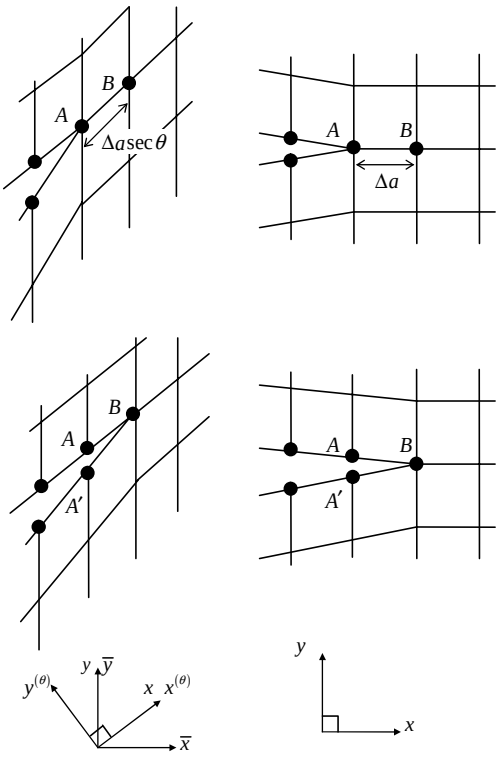

Fig. 13. Plan view of θ-ply crack tip configuration in the finite element model.

ment Δu_i and reaction force F^i at point A obtained from finite element analysis in this study should be transformed to the orthogonal components as

$$\begin{bmatrix} \Delta\bar{u}_A \\ \Delta\bar{v}_A \\ \Delta\bar{w}_A \end{bmatrix} = \begin{bmatrix} 1 & -\sin\theta & 0 \\ 0 & \cos\theta & 0 \\ 0 & 0 & 1 \end{bmatrix} \begin{bmatrix} \Delta u_A \\ \Delta v_A \\ \Delta w_A \end{bmatrix}, \quad \begin{bmatrix} \overline{F}_{xA} \\ \overline{F}_{yA} \\ \overline{F}_{zA} \end{bmatrix} = \sqrt{g} \begin{bmatrix} 1 & 0 & 0 \\ \tan\theta & \sec\theta & 0 \\ 0 & 0 & 1 \end{bmatrix} \begin{bmatrix} F_A^x \\ F_A^y \\ F_A^z \end{bmatrix} \tag{B.1}$$

It should be noted that the contravariant reaction force components have to be compensated by $\sqrt{g}$.

In addition, another orthogonal coordinates are defined as in Fig. 13 in a manner that $x^{(\theta)}$- and $y^{(\theta)}$-directions coincide with the θ-ply fiber and transverse to the fiber directions respectively. Transformation of vector components from the x–y–z orthogonal coordinates to $x^{(\theta)}$–$y^{(\theta)}$–$z^{(\theta)}$ coordinates is expressed as

$$\begin{bmatrix} \Delta\bar{u}_A^{(\theta)} \\ \Delta\bar{v}_A^{(\theta)} \\ \Delta\bar{w}_A^{(\theta)} \end{bmatrix} = \begin{bmatrix} \cos\theta & \sin\theta & 0 \\ -\sin\theta & \cos\theta & 0 \\ 0 & 0 & 1 \end{bmatrix} \begin{bmatrix} \Delta\bar{u}_A \\ \Delta\bar{v}_A \\ \Delta\bar{w}_A \end{bmatrix}, \quad \begin{bmatrix} \overline{F}_{xA}^{(\theta)} \\ \overline{F}_{yA}^{(\theta)} \\ \overline{F}_{zA}^{(\theta)} \end{bmatrix} = \begin{bmatrix} \cos\theta & \sin\theta & 0 \\ -\sin\theta & \cos\theta & 0 \\ 0 & 0 & 1 \end{bmatrix} \begin{bmatrix} \overline{F}_{xA} \\ \overline{F}_{yA} \\ \overline{F}_{zA} \end{bmatrix} \tag{B.2}$$

As the physical crack growth area should be multiplied by $\sqrt{g\,g^{22}}$, energy release rates associated with θ-ply crack growth can be calculated as

$$\begin{aligned} G_{\mathrm{I}} &= \frac{1}{2\Delta A\sqrt{g\,g^{22}}}\overline{F}_{yA}^{(\theta)}\Delta\bar{v}_A^{(\theta)} \\ G_{\mathrm{II}} &= \frac{1}{2\Delta A\sqrt{g\,g^{22}}}\overline{F}_{xA}^{(\theta)}\Delta\bar{u}_A^{(\theta)} \\ G_{\mathrm{III}} &= \frac{1}{2\Delta A\sqrt{g\,g^{22}}}\overline{F}_{zA}^{(\theta)}\Delta\bar{w}_A^{(\theta)} \end{aligned} \tag{B.3}$$

where ΔA denotes crack growth area in the orthogonally-based discrete model and g^{22} is equal to 1 for the oblique coordinate system defined in Eq. (1).

References

Aboudi, J., Lee, S.W., Herakovich, C.T., 1988. Three-dimensional analysis of laminates with cross cracks. Journal of Applied Mechanics 55, 389–397.

Aoki, T., Ishikawa, T., Kumazawa, H., Morino, Y., 2000. Mechanical performance of CF/polymer composite laminates under cryogenic conditions. AIAA Conference Paper 2000-1605.

Flagg, D.L., Kural, M.H., 1982. Experimental determination of the in situ transverse lamina strength in graphite/epoxy laminates. Journal of Composite Materials 16, 103–116.

Garrett, K.W., Bailey, J.E., 1977. Multiple transverse fracture in 90° cross-ply laminates of a glass fibre-reinforced polyester. Journal of Material Science 12, 157–168.

Gudmundson, P., Zang, W., 1993. An analytical model for thermoelastic properties of composite laminates containing transverse matrix cracks. International Journal of Solids and Structures 30, 3211–3231.

Hashin, Z., 1985. Analysis of cracked laminates: a variational approach. Mechanics of Materials 4, 121–136.

Hashin, Z., 1987. Analysis of orthogonally cracked laminates under tension. Journal of Applied Mechanics 54, 872–879.

Henaff-Gardin, C., Lafarie-Frenot, M.C., Gamby, D., 1996. Doubly periodic matrix cracking in composite laminates. Part 1: General in-plane loading. Composite Structures 36, 113–130.

Highsmith, A.L., Reifsnider, K.L., 1982. Stiffness reduction mechanisms in composite laminates. ASTM STP 775, 103–117.

Johnson, P., Chang, F.K., 2001. Characterization of matrix crack-induced laminate failure—Part I: Experiments. Journal of Composite Materials 35, 2009–2035.

Johnson, T.F., Waters, W.A., Singer, T.N., Haftka, R.T., 2004. Thermal-structural optimization of integrated cryogenic propellant tank concepts for a reusable launch vehicle. AIAA Conference Paper 2004-1931.

Kashtalyan, M., Soutis, C., 2000. Stiffness degradation in cross-ply laminates damaged by transverse cracking and splitting. Composites Part A 31, 107–119.

Kumazawa, H., Aoki, T., Susuki, I., 2003. Analysis and experiment of gas leakage through cross-ply laminates for propellant tanks. AIAA Journal 41, 2037–2044.

Lavoie, J.A., Adolfsson, E., 2001. Stitch cracks in constraint plies adjacent to a cracked ply. Journal of Composite Materials 35, 2077–2097.

Masters, J.E., Reifsnider, K.L., 1982. An investigation of cumulative damage development in quasi-isotropic graphite/epoxy laminates. ASTM STP 775, 40–61.

McCartney, L.N., 1992. Theory of stress transfer in a 0°–90°–0° cross-ply laminate containing a parallel array of transverse cracks. Journal of Mechanics and Physics of Solids 40, 27–68.

McCartney, L.N., 2003. Prediction of multiple ply cracking in general symmetric lamimates. In: Proceedings of 14th International Conference on Composite Materials, ASC/SME, San Diego.

McManus, H.L., Maddocks, J.R., 1996. On microcracking in composite laminate under thermal and mechanical loading. Polymers and Polymer Composites 4, 304–314.

Nairn, J.A., Hu, S., 1994. Micromechanics of damage: a case study of matrix microcracking. In: Damage Mechanics of Composite Materials. Elsevier, Amsterdam, pp. 187–243.

Nairn, J.A., 2000. Matrix microcracking in composites. In: Polymer Matrix Composites. Elsevier, Amsterdam, pp. 403–432.

Ogin, S.L., Smith, P.A., Beaumont, P.W.R., 1985. Matrix cracking and stiffness reduction during the fatigue of a [0/90]s GFRP laminate. Composites Science and Technology 22, 23–31.

Robinson, M.J., 1994. Composite cryogenic propellant tank development. AIAA Conference Paper 94-1375-CP.

Schoeppner, G.A., Pagano, N.J., 1998. Stress fields and energy release rates in cross-ply laminates. International Journal of Solids and Structures 35, 1025–1055.

Takeda, N., Ogihara, S., 1994. In situ observation and probabilistic prediction of microscopic failure process in CFRP cross-ply laminates. Composites Science and Technology 52, 183–195.

Tong, J., Guild, F.J., Ogin, S.L., Smith, P.A., 1997. On matrix crack growth in quasi-isotropic laminates—I. Experimental investigation. Composites Science and Technology 57, 1527–1535.

Tsai, C.L., Daniel, I.M., 1993. The behavior of cracked crossply composite laminates under general in-plane loading. In: Damage in Composite Materials. Elsevier, Amsterdam, pp. 51–66.

Yokozeki, T., Aoki, T., 2004. Stress analysis of symmetric laminates with obliquely-crossed matrix cracks. Advanced Composite Materials 13, 121–140.

Zhang, J., Herrmann, K.P., 1999. Stiffness degradation induced by multilayer intralaminar cracking in composite laminates. Composites Part A 30, 683–706.